Results in Materials 20 (2023) 100493

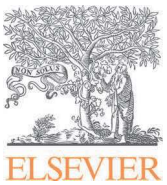

Contents lists available at ScienceDirect

Results in Materials

journal homepage: www.sciencedirect.com/journal/results-in-materials

Static, dynamic and impact properties of a high-performance flax-fiber composite

Ivan Colamartino [a,*], Elia Pinato [b], Matteo Cavasin [c], Marco Tagliabue [c], Marco Anghileri [b], Marco Boniardi [a]

[a] Dipartimento di Meccanica, Politecnico di Milano, Via La Masa 1, Milan, 20156, Italy
[b] Dipartimento di Scienze e Tecnologie Aerospaziali, Politecnico di Milano, Via La Masa 34, Milan, 20156, Italy
[c] Angeloni Group, Via Abbate Tommaso, 72/A – 30020, Quarto d'Altino, VE, Italy

ARTICLE INFO

Keywords:
Flax-fiber composites
Impact mechanics
Crashworthiness
Indentation
Ballistic impact
High strain-rate

ABSTRACT

As environmental issues become increasingly relevant nowadays, the need to develop new materials entirely or partially based on renewable resources is one fundamental step to reduce the consumption of fossil fuels and CO_2 emissions. In that sense, natural fiber composites might represent an environmentally sustainable alternative to conventional solutions such as glass and carbon fiber composites, standard today for many lightweight structural applications; however, solutions are several and diverse in terms of technological process, base materials, mechanical properties, and analysis of their behaviour, necessary for safe industrial use, is still lacking for most resin-fiber combinations. Consequently, this work presents a comprehensive material characterization of a flax-fiber reinforced composite material, analyzing both the static and dynamic mechanical performances, targeting future crashworthiness applications. In particular static tensile, compressive, flexural and shear properties were investigated, while low-speed indentation, high strain-rate tensile and ballistic tests were carried out to probe the dynamic and impact features.

1. Introduction

Composite materials are today standard solutions in many fields, due to their advantages such as low specific weight, high strength-to-weight ratio, resistance to corrosion and fatigue. Composites were capable of satisfying the market of lightweight high-performance structures market demand for several decades, especially in automotive and aerospace field. However, the industry needs changed over the past few years and new needs must be satisfied. At the actual rate of consumption, the world petroleum resources are in fact estimated to last only for the next 50 years or so [1]. Environment-aware laws and regulations are consequently getting stricter, leading to increasing disposal costs of synthetic composite materials and forcing the industry to look at more sustainable alternatives for current and future applications.

In this context, natural composite materials may be able to meet these needs by exploiting their most relevant benefit: biodegradability. Benefits are found in all the phases of the production process: plantation, mostly based on human workforce in developing countries and as such an economic opportunity for those countries, intrinsically reducing CO_2 emissions and on the contrary emitting oxygen; manufacturing, much less polluting with respect to synthetic composites'; recyclability or biodegradability, partial or full as a function of the material. In terms of structural properties natural fiber composites feature lower perfomances with respect to standard petroleum-based solutions, while are also more threatened by environmental conditions such as high temperatures and humidity [2]. However such disadvantages, considered in perspective of the new industry demands, are compensated with biodegradability, low cost and large availability of natural raw materials, advantages in production costs and sustainability.

Historically, natural materials have been employed for the production of non-structural car components; in particular, car interiors such as seat backs, parcel shelves, front and rear door coating, trunk coating, and door-trim panels were fabricated with plant reinforced composites [3]. Today, although traditional composites are still the best solution for most lightweight structural applications, first attempts to design structural components with natural fiber composites have been performed: one notable example is an aircraft wing box made of ramie fiber composites, revealing a 12/14 % decrease in weight [4]. A comprehensive

* Corresponding author.
E-mail address: ivan.colamartino@polimi.it (I. Colamartino).

https://doi.org/10.1016/j.rinma.2023.100493
Received 21 October 2023; Received in revised form 14 November 2023; Accepted 16 November 2023
Available online 27 November 2023

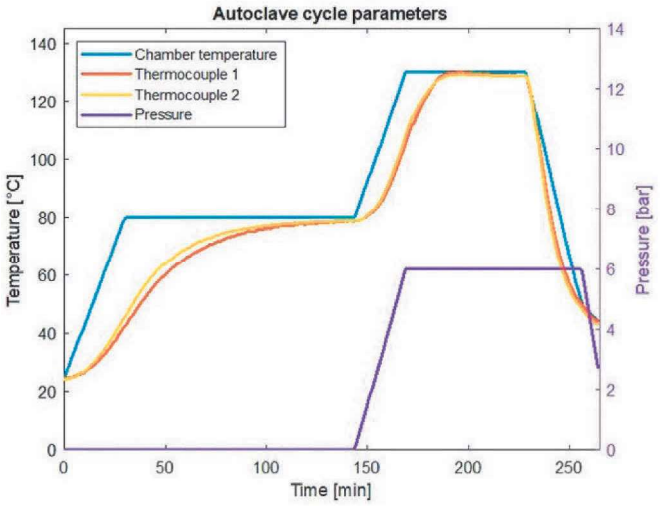

Fig. 1. Curing cycle.

review the natural fiber composites and their applications may be found in Ref. [5].

In the field of impact mechanics, investigative studies with promising results have been conducted in recent years. For example, crashworthiness characteristics have been studied on natural silk-epoxy rectangular tubes [6], on carbon-jute-glass-epoxy composite circular tubes [7], and comparison amongst hemp-epoxy, flax-epoxy and jute-epoxy composite cones have been conducted [8]. It was also reported that natural materials present superior damping properties for low and mid-frequency regions during crash scenarios [9]. However, literature still lacks proper experimental characterization of most resin-fiber combinations, especially for what concerns impact and dynamic properties.

Consequently, in the present work a promising natural fiber composite, a flax-fiber twill pre-impregnated produced by Angeloni Group and making use of Bcomp ampliTex™ fibers, is studied targeting crashworthiness applications. First, a comprehensive static characterization is carried out to provide a complete overview of its mechanical properties; tyipcal composite testing methods are used for best reproducibility: static tensile, compressive, flexural, shear. Subsequently, strain rate sensitivity is studied by means of a dynamic tensile testing campaign, with the purpose of evaluate the in-plane behavior at deformation rates most frequently encountered in crashworthiness applications. Then, out-of-plane resistance is evaluated at low impact speeds with indentation tests and at high impact speeds with ballistic tests, in order to provide a suited outline of the behavior of the present flax-fiber composite in terms of resistance to threats such as minor collisions during manufacturing, or high-speed impacts such as debris, ice.

2. Materials and methods

2.1. Manufacturing

The selected natural composite material was the flax-fiber pre-impregnated Impregnatex APX 300T IMP503Z-HT BC 44, a 300 gsm (grams per square meters) 2 × 2 twill with density of 1.33 g/cm^3.

The production, performed by Angeloni Group, was achieved through the autoclave vacuum-bag moulding process, one of the oldest and most versatile manufacturing methods for composite components, known to offer composites with high mechanical features and good quality surface. On the other side, the workers' skill and know-how are essential to properly perform every step of the procedure. Eventually, the method is time-consuming but suitable for low production volume and as such was the most suited for the objectives of the present work.

The cure cycle consisted in the following steps:

1. Vacuum applied and checked;
2. 2 °C/min heating ramp;
3. 45 min stasis at 80 °C;
4. 2 °C/min heating ramp, 0.25 bar/min;
5. 45 min stasis at 130 °C, 6 bar;
6. Controlled cooling down, final pressure release.

Two thermocouples were placed on the cold spots of the caul plates to ensure that the plies reached the correct stasis temperature, which is critical for proper resin curing. The implemented cycle is showed in Fig. 1.

At the end of the procedure three different laminates were obtained, two of them were characterized by a 6-ply layout, one with 8-ply layout, one with 12-ply layout; lamination sequences will be detailed later on in the document. Laminates were cutted trhough a ProtoMAX abrasive waterjet cutter in order to avoid damages to the fibers.

Within manufacturing a first testing campaign, a Dynamic

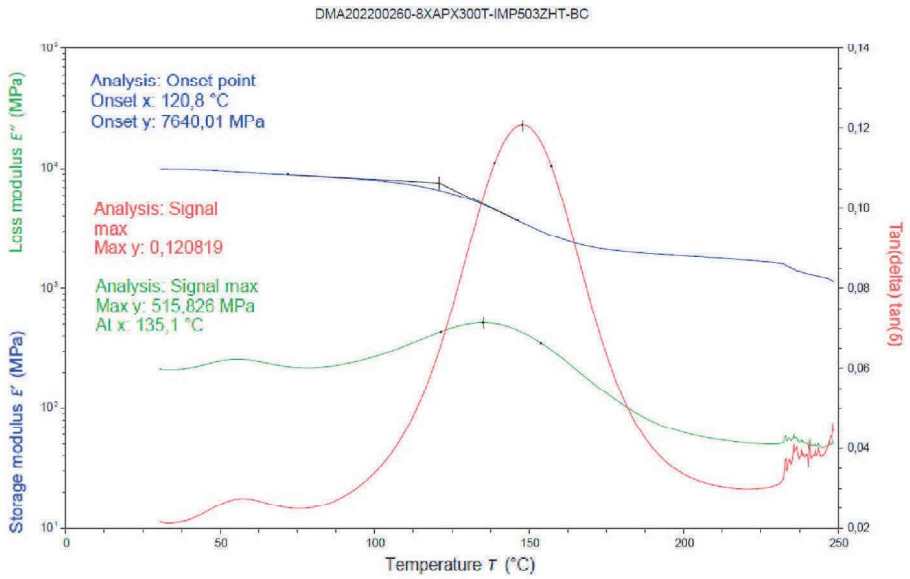

Fig. 2. Dynamic Mechanical Analysis results.

Table 1
Specimens – tensile test D3039.

Specimen ID	Length [*mm*]	Width [*mm*]	Thickness [*mm*]
APX300_0_1-8	250.31 ± .91	25.01 ± .05	2.34 ± .02
APX300_90_1-6	251.15 ± .68	25.00 ± .03	2.36 ± .03

Table 3
Specimens – bending test D790.

Specimen ID	Length [mm]	Width [mm]	Thickness [mm]
APX300_0_1-8	119.57 ± .46	15.00 ± .43	2.32 ± .04

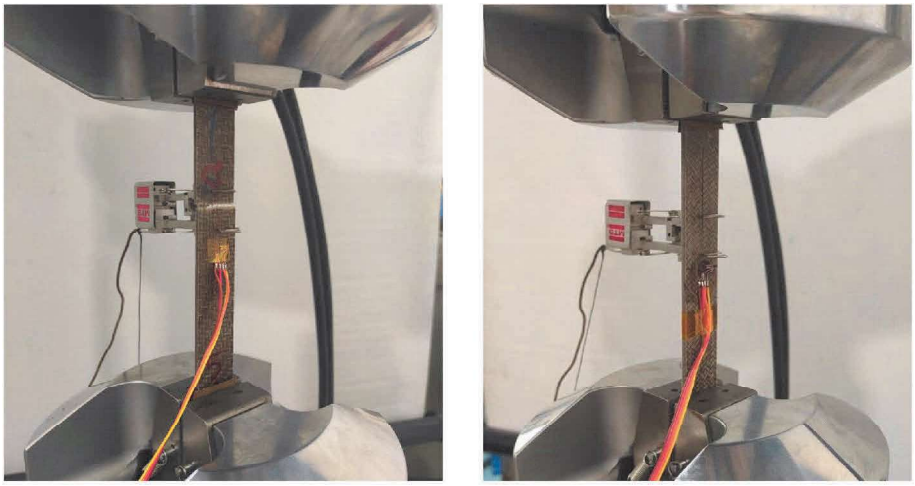

Fig. 3. Tensile (left) and shear test (right) – setup.

Table 2
Specimens – shear test D3518.

Specimen ID	Length [*mm*]	Width [*mm*]	Thickness [*mm*]
APX300_45_1-6	250.04 ± .93	25.03 ± .04	3.16 ± .04

Table 4
Specimens – compressive test D6641.

Specimen ID	Length [mm]	Width [mm]	Thickness [mm]
APX300_0_1-15	139.98 ± .23	16.08 ± .04	2.34 ± .05

Mechanical Analysis (DMA), was performed to grasp the viscoelastic properties of the composite as a function of temperature. Results of the 6-ply laminate are reported in Fig. 2.

In detail, storage modulus (E′) represents the elastic portion, loss modulus (E″) represents the viscous part and δ represents the phase lag between stress and strain and can be defined as: $\delta = \text{atan}(E''/E')$. From the storage modulus the glass transition temperature T_g is calculated, reported at 120.8 °C. However, it must be noted that changes in the physical features were exhibited from about 75 °C, as shown by the small changes in the slope of E”.

2.2. Static tests

The static tests selected to conduct the material characterization, all complying to the American Society for Testing and Materials (ASTM) standards, were the following:

- tensile test, ASTM D3039 [10];
- compression test, ASTM D6641 [11];
- shear test, ASTM D3518 [12];
- three-point bending test, ASTM D790 [13].

To assure the statistical validity of the tests at least five samples were tested for each campaign. To guarantee repeatable environmental and sample conditions, an industrial oven was employed before each test: samples were heated up to 60 °C for at least 2 h to limit the amount of moisture content. Static tests were conducted with two different machines: MTS 858 for bending test and MTS 370.10 for all the remaining

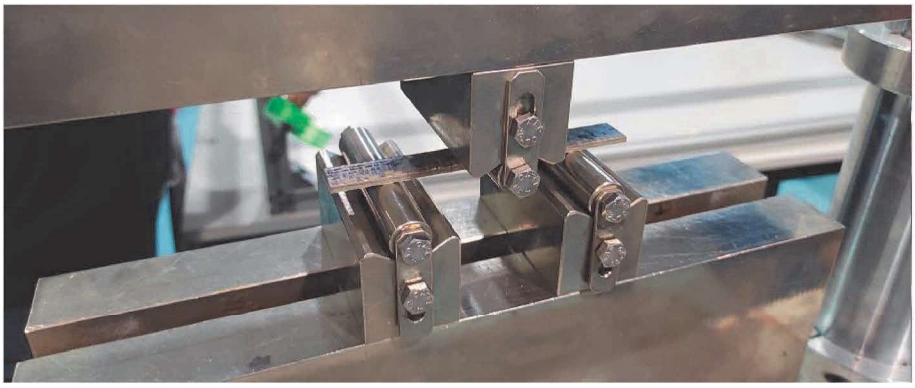

Fig. 4. Bending test – setup.

(a) Sample support (b) Falling impactor

Fig. 5. Dynamic tensile test – test rig.

Table 5
Specimens – dynamic tensile tests.

Specimen ID	Length [*mm*]	Width [*mm*]	Thickness [*mm*]
APX300_0_1-9	164.95 ± .20	9.40 ± .03	2.35 ± .02
APX300_0_1–6_SG	165.04 ± .04	15.13 ± .03	2.37 ± .02

type of tests, acquiring for both cases vertical load and crosshead displacement. For what concerns the testing speed, all specimens were tested with fixed displacement rate of 1 mm/min, except for the compression's, fixed at 0.5 mm/min to better comply to the lower gauge length. In cases were an accurate measurement of the local strain was needed, specimens were equipped with strain gages: a biaxial KYOWA KFGS-3-350-D16-11 for tensile and shear tests and a uniaxial KYOWA KFGS-3-350-C1-11 for compressive tests. In addition, the axial extensometer MTS 634.31F-24 was used to guarantee redundancy and extend the results to specimens not equipped with strain gages. Samples' names, valid also for the dynamic tests, are reported as "<material name>_<fibers orientation>_<specimen number>"; for instance, "APX300_0_1″ identifies sample number 1, made of ampliTex 300 with 0-degrees fiber orientation. For samples' measurements, a digital caliper with a resolution of 0.01 mm and precision of 0.03 mm was employed, measuring in multiple points and averaging the values obtained for each dimension.

It's worth noting that characterization performed and hereby reported was focused on the macroscopic static and dynamic properties of the laminates. Nonetheless, it is known that the thermo-physical features of composites are of notable importance in determining their mechanical behavior, especially when natural fibers are used [14]. However, testing activities for evaluation of moisture absorption, void volume, and chemical properties are not reported here nor were performed in the present work; instead, all the feasible countermeasures were taken to assure limited contributions of these issues, most of all the proper heating mentioned above and applied immediately before any testing campaign.

2.2.1. *Tensile test – D3039*

This test method is designed to produce in-plane tensile properties of polymer matrix, fiber-reinforced composite materials. Thin rectangular flat specimens of material of nominal dimensions of 250 × 25 × 2.3 mm are mounted on the grips of a mechanical testing machine and axially loaded in tension until failure, as prescribed by the ASTM D3039 standard [10].

The employed specimens and their sizes are reported in Table 1. In

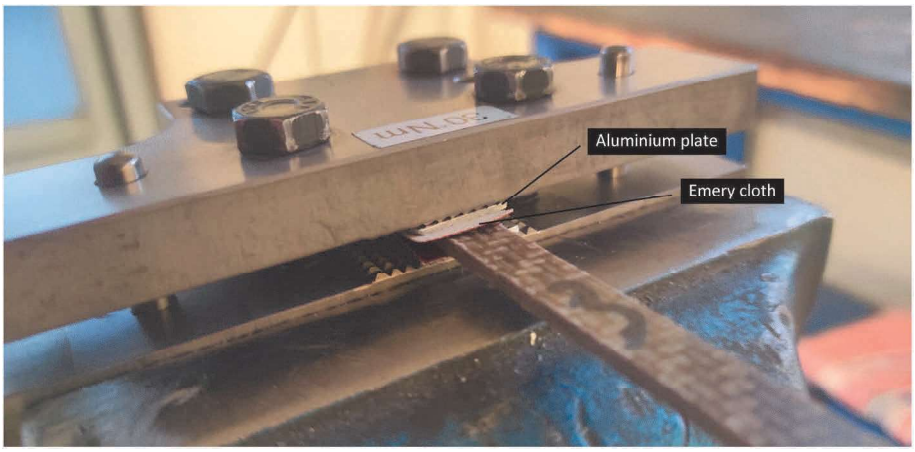

Fig. 6. Dynamic tensile test – test rig.

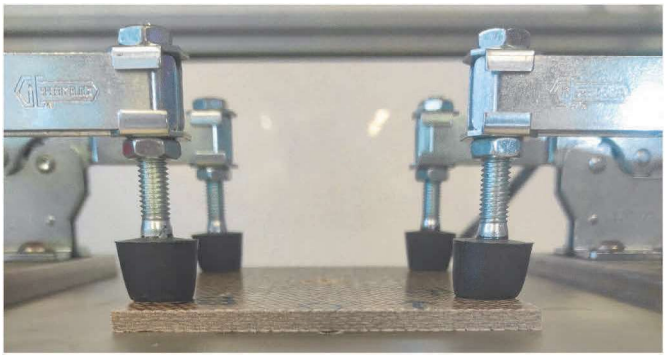

Fig. 7. Indentation test – fixture

Table 6
Indentation test – setup.

Impactor	Diameter [mm]	Impactor mass [g]	Total sled mass [kg]
D127	12.7	171.0	10.0228
D16	16.0	242.0	10.0938
D20	20.0	227.6	10.0794

Table 7
Specimens – indentation test.

Specimen ID	Length [mm]	Width [mm]	thickness [mm]
APX300_mix_-	150.32 ± .98	100.42 ± .60	4.95 ± .21

woven composites, warp and weft directions usually exhibit different mechanical features: due to manufacturing process, it was observed in previous experience that warp direction (0°) tends to show slightly better performance than weft direction (90°). Hence, both orientations were considered during the test campaign.

The test setup is presented in Fig. 3a. As shown, the sample was equipped with both a the biaxial strain gage and an extensometer. The specimen was directly clamped at both ends by wedge-shaped grips. As the load can be properly transferred due to the presence of coarse emery cloth, the presence of tabs was not required.

Table 8
Specimens – high-speed test.

Specimen ID	Length [*mm*]	Width [*mm*]	Thickness [*mm*]
APX300_mix_1	122.31 ± .21	100.25 ± 1.51	4.96 ± .03

Other than the stress strain curve, main output parameters were ultimate tensile strength and strain: the first was calculated as the ratio between the maximum applied forced recorded by the machine and the cross-sectional area of the specimen (Equation (1)), the second (Equation (2)) by taking as l_0 the crosshead displacement, the extensometer measure or the strain gage measure.

$$\sigma_{max} = F_{max}/A \tag{1}$$

$$\epsilon = \Delta l/l_0 \tag{2}$$

Other paremeters of interest are the modulus of elasticity, calculated as per Equation (3) between 1000 and 3000 $\mu\varepsilon$ as prescribed by the norm, and the Poisson ratio (Equation (4)), computed over the same strain range.

$$E_1 = \Delta\sigma/\Delta\epsilon \tag{3}$$

$$\nu_{12} = \epsilon_{\perp}/\epsilon_{\parallel} \tag{4}$$

2.2.2. Shear test – D3518

The test method evaluates the in-plane shear response of polymer matrix composite materials as regulated by the ASTM D3518 standard [12]. The set-up, shown in Fig. 3b is similar to test method D3039 applied for tensile tests, the differences are in samples stacking sequence and sizes: a 250 × 25 × 3 mm laminate ±45° balanced and symmetric (Table 2).

From the in-plane shear stress versus shear strain chart, information such as shear modulus, maximum shear stress and maximum shear strain can be achieved. In order to draw such graph, in-plane shear stress can be defined as reported in Equation (5), where F is the applied force and A is the section area. The shear strain can be described as per Equation (6), where ε_x and ε_y are respectively the longitudinal and transverse strains measured by the biaxial strain gage sensor applied on the specimen. Subscripts 1–2 represent the lamina directions, whereas x-y are referred to laminate directions. The shear modulus of elasticity is

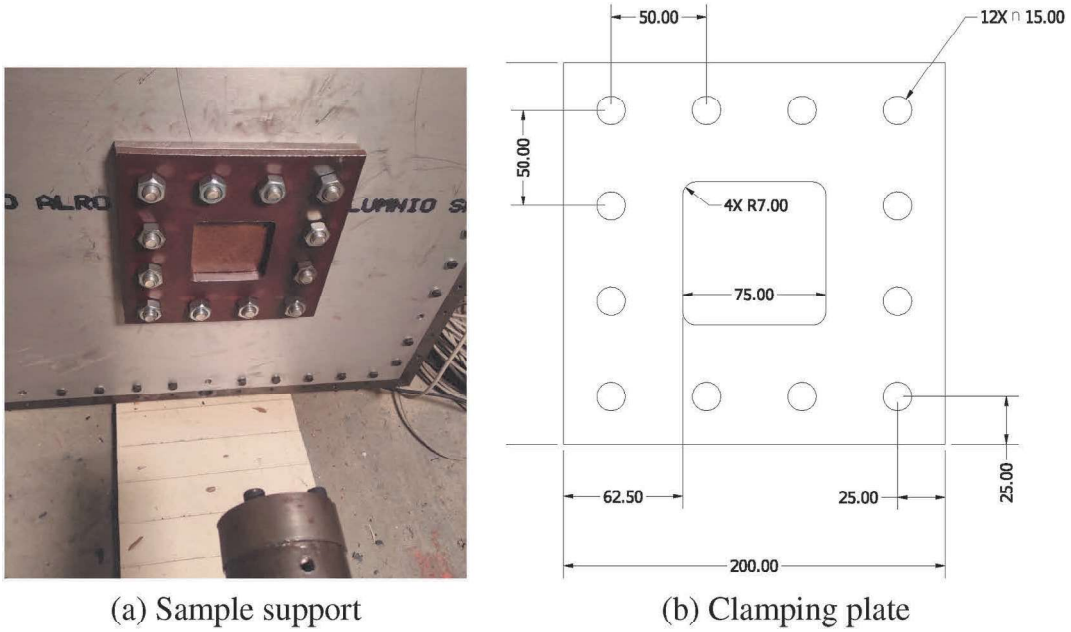

Fig. 8. Dynamic tensile test – test rig.

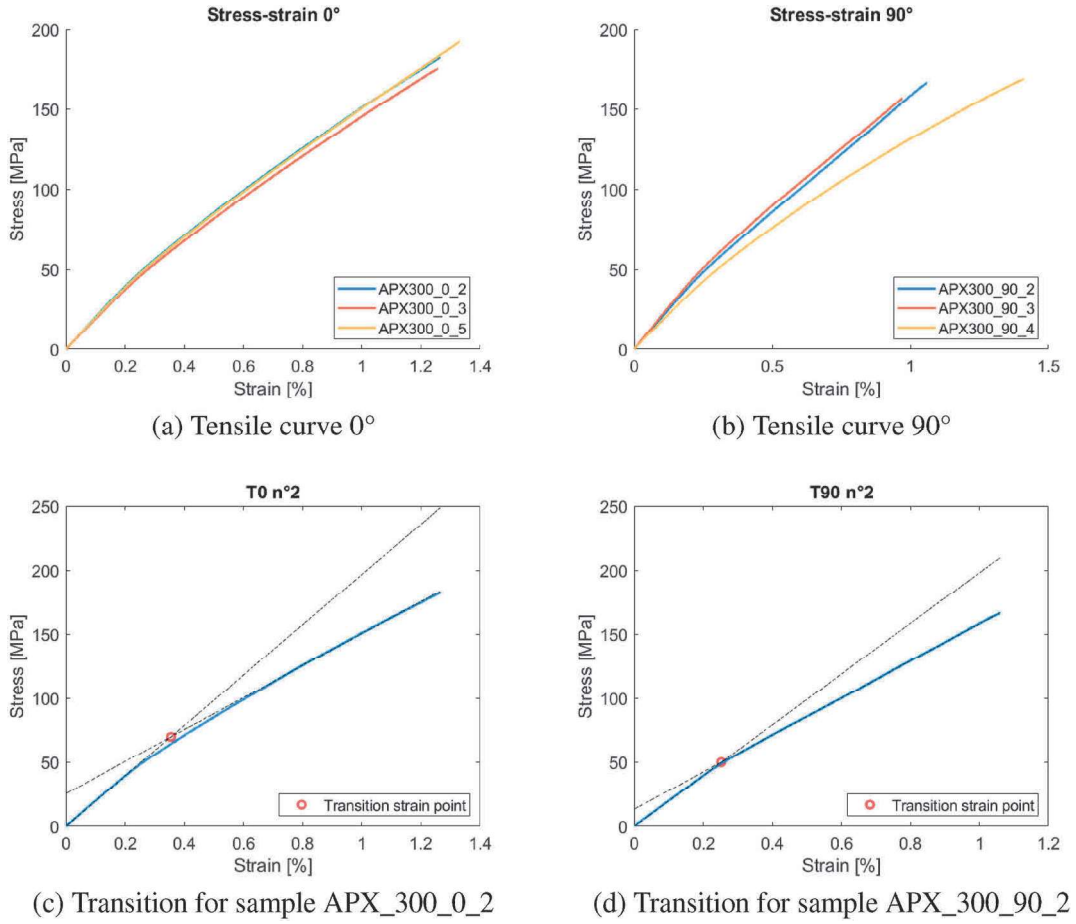

(a) Tensile curve 0° (b) Tensile curve 90°

(c) Transition for sample APX_300_0_2 (d) Transition for sample APX_300_90_2

Fig. 9. Static tensile test – results.

Table 9
Static tensile 0° – test results.

-	$\sigma_{1_{max}}$ [MPa]	E_1 [MPa]	$\epsilon_{1_{max}}$ [−]	ν_{12} [-]	$\epsilon_{1_{transition}}$ [−]
Avg.	181.3900	17.7300	1.2800	0.1300	0.3500
Std. Dev.	5.8400	0.4600	0.0400	0.0600	0.0040
Coeff. of variation [%]	3.22	2.62	3.14	45.62	1.01

Table 10
Static tensile 90° – test results.

-	$\sigma_{2_{max}}$ [MPa]	E_2 [MPa]	$\epsilon_{2_{max}}$ [−]	ν_{21} [-]	$\epsilon_{2_{transition}}$ [−]
Avg.	161.6900	17.8700	1.1500	0.1500	0.3100
Std. Dev.	7.3000	1.4500	0.2300	0.0100	0.0800
Coeff. of variation [%]	4.52	8.11	20.23	7.57	26.25

then calculated as reported in Equation (7).

$$\tau_{12} = F_x/2A \tag{5}$$

$$\gamma_{12} = \epsilon_x - \epsilon_y \tag{6}$$

$$G_{12} = \frac{\sigma_x}{2(\epsilon_x - \epsilon_y)} \tag{7}$$

where $\sigma_x = F/2A$ is the longitudinal stress. The shear modulus is then evaluated between 2000 and 6000 $\mu\varepsilon$, interval chosen re-calculating the range used for tensile test assuming a Poisson's ratio near to 1. The ultimate in-plane shear stress is achieved considering the maximum load at or below 5 % shear strain; if a maximum stress value is recorded at strain values over 5 %, the maximum shear stress is evaluated at $\varepsilon = 0.05$.

Table 11
Shear test – D3518 – test results.

-	$\tau_{12_{max}}$ [MPa]	$\gamma_{12_{max}}$ [%]	G_{12} [GPa]
Avg.	46.2100	4.7100	1.9600
Std. dev.	0.4600	0.2500	0.0600
Coeff. of variation [%]	0.99	5.29	2.89

2.2.3. *Bending test – D790*

Out-of-plane properties were characterized through bending test method according with ASTM D790 standard [13]. The test is performed on a 3-point-bending setup, as presented in Fig. 4.

The specimen, a flat rectangular laminate of nominal dimensions 120 × 15 × 2.3 mm (Table 3) is simply supported by two rigid cylinders with diameters of 15 mm and is loaded by means of a third cylindrical nose midway between the supports; the loading span was 75 mm, accordingly to a 32:1 ratio as presecribed by the norm.

The flexural stress is calculated as follows:

$$\sigma_f = \frac{3FL}{2bt^2}\left(1 + \frac{D^2}{L^2} - 4\frac{t}{L}\frac{D}{L}\right) \tag{8}$$

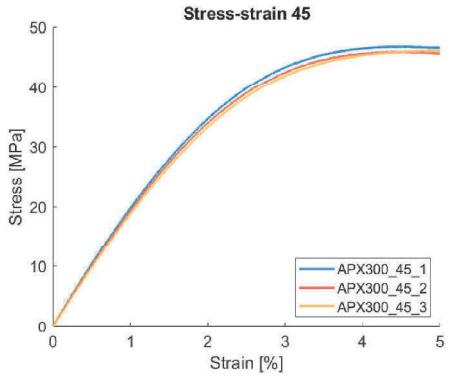

Fig. 10. Shear test – results.

Table 12
Bending test – D790 – test results.

-	$\sigma_{f_{max}}$ [MPa]	$\epsilon_{f_{max}}$ [%]	E_f [GPa]
Avg.	199.80	1.86	15.95
Std. dev.	12.40	0.12	0.44
Coeff. of variation [%]	6.21	6.58	2.74

where F is the applied force, L the span distance, b the specimen width, t the specimen thickness, D the loading nose vertical displacement. Due to the orthotropic nature of flax composite fabric, shear deflection may have seriously reduced the apparent modulus of elasticity, hence the tangent modulus was considered:

$$E_B = \frac{3m}{4bd^3} \tag{9}$$

where the parameter m represents the slope of the tangent to the initial portion of the load-deflection curve. As for the tensile test, a range in between 1000 and 3000 $\mu\varepsilon$ is used to perform the calculus.

2.2.4. Compressive test – D6641

This test method determines the in-plane compressive properties of natural composite materials by means of a combined loading compression test fixture. The used ASTM D6641 standard [11] applies the compressive load on the specimen through a combination of shear and axial forces to prevent instability; with respect to the more common test method D3410 [15] where a pure shear-loading is used and instability is more likely to occur. The test method setup is analogous to tensile test method, with a loading acting in compression. The specimen geometries reported in Table 4 were in compliance with the standard, but a larger value of thickness was chosen with respect to the suggested (1.5 mm) to minimize instability phenomena during the test: consequently, the provided samples were able to give consistent results while avoiding the instability phenomena.

The compressive modulus of elasticity is obtained through equation (3) used for tensile, and the same strain range between 1000 and 3000 $\mu\varepsilon$ was used for its computation. In order to evaluate the strain value and guarantee control over the induced bending, two axial strain gages were employed on both the surfaces of the specimen, and the following equation was exploited to calculate the bending fraction:

$$B_y = \frac{\epsilon_1 - \epsilon_2}{\epsilon_1 + \epsilon_2} \tag{10}$$

This parameter can be affected by imperfections in test specimen, test fixture, and even testing procedure. Eventually, the evaluation of the strain consists in an average between the measurements given by the two sensors applied on both sides. By means of Equation (1) the ultimate compressive stress value can be evaluated.

2.3. Dynamic tests

In order to evaluate the dynamic response of flax composite material three experimental campaigns were performed: high strain-rate tensile to study the sensitivity to strain rate, ASTM D7136 [16] low-speed indentation with three different indenters and ballistic test for evaluation of the out-of-plane behavior from low to high energies.

The first two dynamic tests were performed exploiting a Step Lab DW1000 drop tower. Such machine employs high-performant load cells sampled at high frequencies for optimal measurement accuracy. Some of the specimens of the dynamic tensile campaign were further equipped with uniaxial strain gages, in order to accurately compare stress-strain dynamic behaviour with static results. The third campaign was carried out with a dedicate gas gun, capable of range of speeds between 20 and 200 m/s. Out-of-plane tests were followed by visual inspection of the post-impact damage to extract the failure mode.

2.3.1. Dynamic tensile test

This test aims to investigate the strain rate dependency, obtaining the variation of the tensile properties at increasing deformation rates. Low deformation rates (40–100 s^{-1}) were analyzed here, as crashworthiness properties are evaluated in the present document.

In order to execute the test the lower part of a flat rectangular specimen is clamped to a T-shaped grip, free to move, while the upper part is clamped to a rigid support equipped with a force sensor, in the present case a Dytran 1210V4. The tensile dynamic load is applied

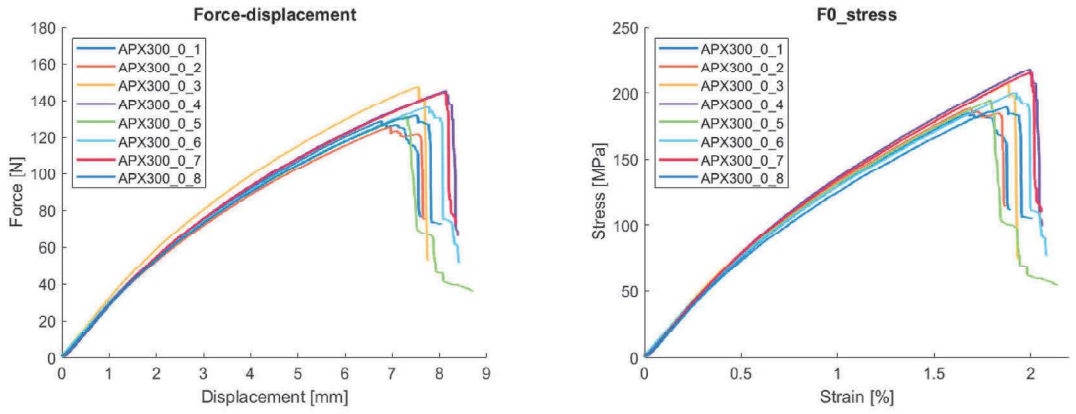

(a) Force vs displacement (b) Stress vs strain

Fig. 11. Bending test – results

Table 13
Compression 0° – test results.

-	$\sigma_{1_{max}}$ [MPa]	E_1 [MPa]
Avg.	141.57	15.04
Std. Dev.	5.10	0.69
Coeff. of variation [%]	3.61	4.60

Table 14
Compression 90° – test results.

-	$\sigma_{2_{max}}$ [MPa]	E_2 [MPa]
Avg.	141.53	15.02
Std. Dev.	0.85	0.10
Coeff. of variation [%]	1.00	0.69

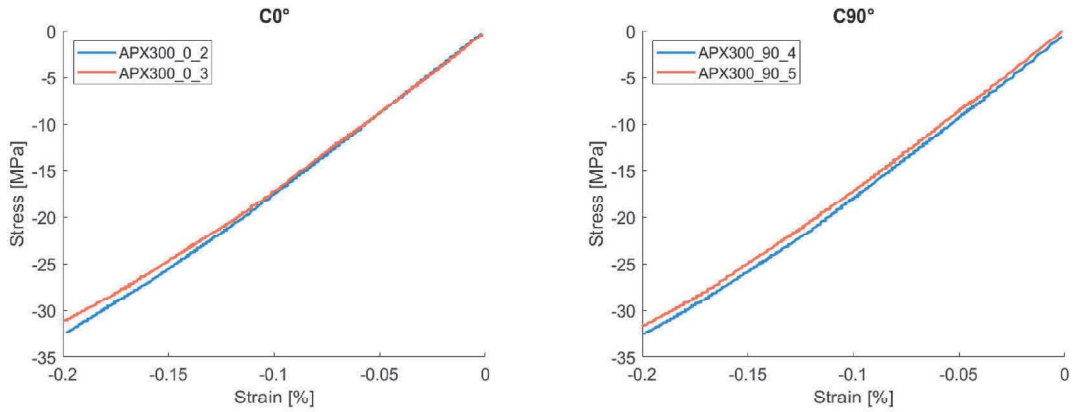

(a) Stress vs strain (b) Stress vs strain

Fig. 12. Compressione test – results.

through a falling mass mounted on a vertical sled, released from the designed height, impacting the lower grip and quickly tearing the specimen. Clarifying pictures are shown in Fig. 5.

The geometry of the employed samples is reported in Table 5; specimens were manufactured using woven fabric prepreg with 0° oriented fibers (warp direction), in order to inspect the higher mechanical performances; other directions were left for future developments. Due to the complexity of the test, a total of 15 samples with two different widths were used, both for proper test design and output analyses; of these samples, four specimens presented a compliant[1] failure and only these are reported in the results 3.2.1.

It is important to highlight that specimens were devoid of tabs as for the static tensile tests; however, the loading condition is much more severe and countermeasures for limiting propagation of undesired local high-stress regions were necessary. In fact, grips are toothed, T-shaped hard steel plates, kept together by four M6 bolts to be tightened at a suggested value of 30 Nm; a peculiar clamping common in similar apparatuses due to its compact assembly. However, though theoretically symmetric and even if carefully applied, this solution is far from the optimal clamping guaranteed by typical wedge grips used for static tensile tests: first, because tightening torque application is inevitably asymmetric; second, because the suggested torque of 30 Nm is not valid for any material, but depends on the specimen stiffness and hardness and must be consequently calibrated in pre-testing phase. The issue is further amplified by the impulsive loading condition, inducing locally high-frequency peaks. As a consequence, most of the samples were initially discarded for breakage along the grip line. To solve the problem, a new method is proposed: the application as tabs of one layer of emery cloth and one thin aluminium plate between the sample and the grip, as shown in Fig. 6. Such method, applied together with a optimized tightening torque of 25 Nm, proved to be successful, as shown from the results reported in Section 3.2.1.

In the calculation of the strain rate hardening law, failure stress at multiple values of nominal strain-rate $\dot{\epsilon}_0$ were evaluated as follows (Equation (11)):

$$\dot{\epsilon}_0 = \frac{v_0}{L_0} \tag{11}$$

where v_0 and L_0 are respectively impact speed and gage length.

2.3.2. Indentation test – D7136

Out-of-plane indentation resistance is investigated through the application of ASTM D7136 standard [16]. Flat squared specimens were clamped in four points with a dedicated fixture to ensure proper fixation and prevent in-plane displacement (Fig. 7); the test is then carried out with a drop tower loaded with a total of 9.852 kg ballast mass, with tree different hemispherical striker tips used as impactors (Table 6).

In Table 7 the specimens' geometry is reported in compliance with the D7136 standards. A thickness value in between 4 and 6 mm is required to guarantee proper failure mode; consequently, 12 plies were laminated with a symmetric stacking sequence, $[+45/-45/0/90]_{3s}$. In the present document, the code associated to this stacking sequence is "mix", as such related samples are named "<material name>_mix_<specimen number>".

The damage resistance properties obtained with this test method are highly dependent upon several factors such as impactor geometry, impacting mass and energy: for this reason, for each impactor tip at least three values of impact energy were evaluated.

2.3.3. High speed test

The ballistic test campaign was performed to investigate the out-of-plane behaviour under high-velocity impact events, with purpose of evaluating the composite's resistance to debris impact. In order to execute the test, the gas gun facility at LaST was employed, with steel spherical bullets of 18 mm diameter and mass of 23.7 g. Samples of dimensions 100 × 75 mm and same stacking sequence as for the indentation tests were clamped to a rigid support composed of two 10 mm thick holed square plates, fixed by means of M10 bolts to a rigid support perpendicular to the shooting trajectory. Clarifying pictures of the setup and drawings of the clamping plates are shown in Fig. 8,

[1] As the present test method is a non-standard procedure, compliance is intended as for the respective static test, i.e. a rupture within the gage section.

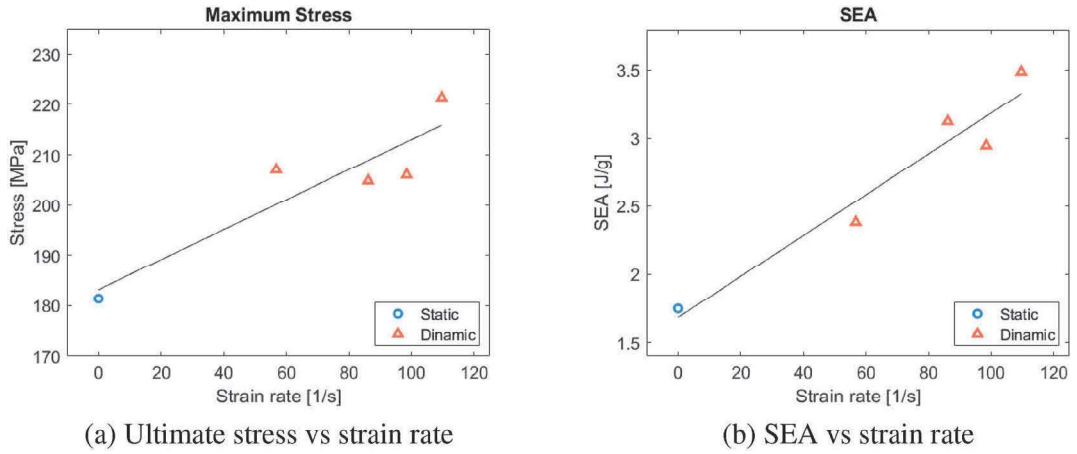

(a) Ultimate stress vs strain rate (b) SEA vs strain rate

Fig. 13. Dynamic tensile test – results

Table 15
Indentation test results. Cases with IDs 20 and 17 did not feature any acquired data: as such, energy values are to be intended as nominal.

ID	Impactor	Impact energy [J]	Absorbed energy [J]	Damage type
19	D127	9.7	8.60	BV
21	D127	14.5	13.77	PP
15	D127	25.8	19.27	FP
20	D16	8.0	–	BV
3	D16	8.7	8.36	BV
17	D16	20.0	–	PP
14	D16	25.4	18.13	FP
18	D16	30.3	23.36	FP
4	D20	10.3	11.16	BV
7	D20	16.2	14.91	BV
16	D20	25.8	22.63	PP
5	D20	35.1	29.28	FP

samples' specifics are reported in Table 8.

Measured test parameters were input and eventually exit speed, evaluated through Digital Image Correlation (DIC) by means of two independent high-speed Phantom VEO-E 310L, mounted perpendicular to the trajectory; for each test, at least 3 different measures were collected to minimize the measurement error.

3. Results and discussion

3.1. Static tests

3.1.1. Tensile test – D3039

Results of the tensile tests are reported for both the 0° oriented samples and 90° oriented samples in Fig. 9 and Tables 9 and 10.

Despite the woven characteristics of the laminates, a difference in the mechanical performances between the two fibers directions is evident: in particular, the 0° oriented samples show better ultimate tensile stress. The results is common in woven composite, and the reason is found within manufacturing: to produce prepregs, weft fibers are maintained straight and pulled, while warp fibers are inserted and consequently slightly bent, inevitably causing minor drops in mechanical properties; however, values reported here are much higher than what is commonly found for carbon or glass fiber composites, suggesting higher sensitivity of flax-fiber composites to the fabric type with respect to standard solutions.

Other peculiarity of natural fiber composites is a bi-linear elastic trait, due to a so-called *transition region* [17] identified by a transition value of strain, where the elastic modulus decreases of few tens percent. In that sense, the present material makes no exception, as a transition point is clearly identified between around 30–35 % strains for both weft and warp directions. Transition for specimens APX300_0/90_2 are shown in Fig. 9.

For what concerns the 0° direction, standard deviation were low in all cases except for the Poisson ratio, evaluated at 0.13 ± 0.06; such uncertainty is likely caused by minor defects in the measurements of biaxial strain for specimen APX_300_0_5, whose removal adjusts the

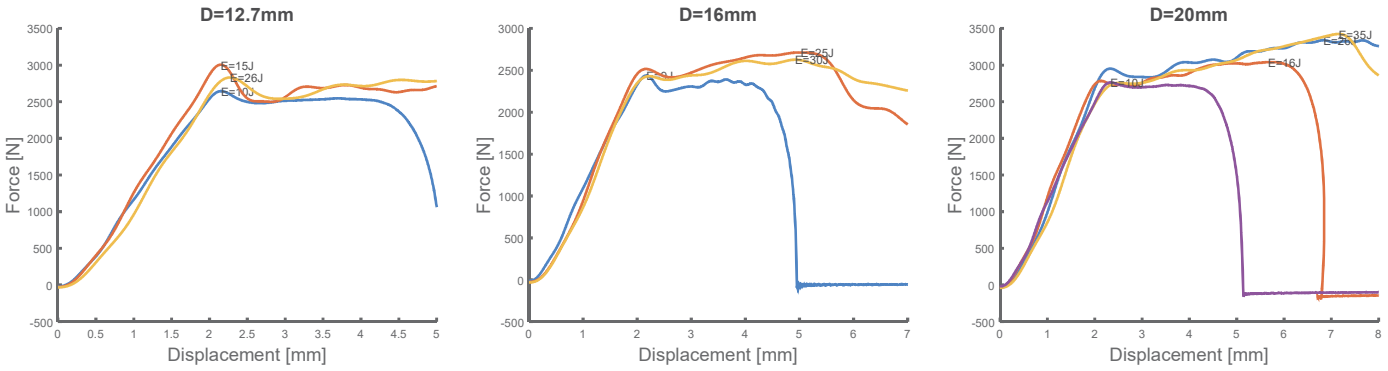

(a) Force vs displacement (b) Force vs displacement (c) Force vs displacement

Fig. 14. Indentation test, force vs displacement curves; the displacement is calculated through a time-integration of the force signal.

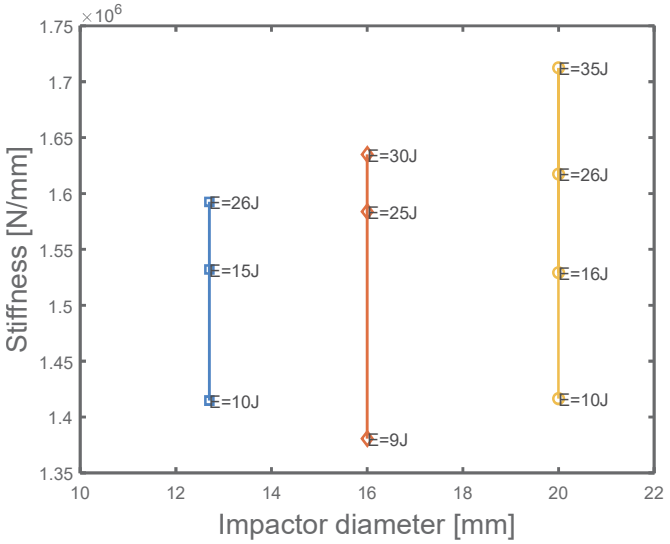

Fig. 15. Indentation test – stiffness analysis

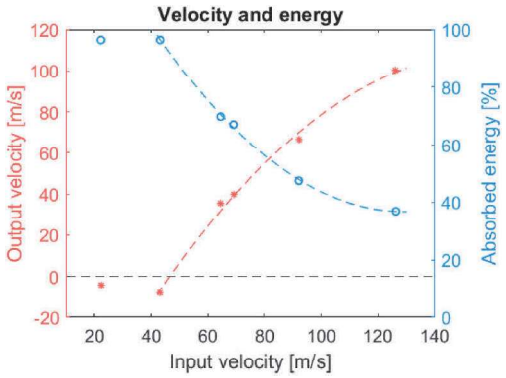

Fig. 16. High speed test – input vs output speed and absorbed energy.

result to $\nu_{12} = 0.15 \pm 0.01$. The low variation reported for $\nu_{21} = 0.015 \pm 0.01$ (7.5 %) on the 90° direction test confirms the validity of such removal (Equation (12)):

$$\nu_{12} = \frac{E_1}{E_2}\nu_{21} = \frac{17.73}{17.87} * 0.15 = 0.15 \tag{12}$$

Results for the 90° direction presented averagely higher values of standard deviations. In particular a 20 % uncertainty was reported over the failure strain, with a larger scatter evident in the three tested samples 9, as well as the transition failure point.

In terms of failure analysis, 0° samples showed homogeneous results with breakage point within the gage sections; on the contrary, even if global stress and strain failure values were consistent throughout all the tests, two 90° samples did not exhibit compliant failure and were consequently discarded. In general, extraction of coherent result in 90° tests appeared to be more difficult, reporting larger scatters and higher sensitivity to specimens' defects, especially towards failure.

3.1.2. Shear test – D3518

Results of the shear tests are reported in Table 11 and Fig. 10.

Satisfactory results were reported for all the specimens, with maximum variations at 5.3 % for the failure point, and typical non-linear curve commonly found for similar cases.

3.1.3. Bending test – D790

Results of the bending tests are reported in Table 12 and Fig. 11; all specimens failed in compliance to the D790 standard. As common in similar cases, it's worth noting that most of the specimens were able to carry a portion of the load even after reaching the maximum stress peak, thanks to the undamaged plies in the laminate and as notable by the step-shaped curve after the peak: force eventually dropped to zero when all the plies have failed.

As for the shear tests, coefficient of variations for all the notable parameters were low, with maximum reported at 6.7 % for the failure strain.

Table 16
High speed test results. Case 2 does not present an exit speed value due to data loss during acquisition.

ID	Input speed [m/s]	Exit speed [m/s]	Absorbed energy [J]	Absorbed en. [%]
1	92.00	66.67	47.55	47.48
2	22.25	–	–	–
6	69.11	39.68	37.88	67.03
8	43.22	−8.22	21.31	96.38
9	126.16	100.20	69.55	36.93
11	64.51	35.47	34.35	69.76

3.1.4. Compression test – D6641

Results of the compression tests are shown in Tables 13 and 14 and Fig. 12.

Coefficients of variations were amongst the lowest for the reported static tests, with maximum at 4.6 %, the elastic modulus at 0°. However, as mentioned in Section 2.2.4, this test method is highly sensitive to specimen geometry, manufacturing defects, fiber orientation and improper alignment: it's then fundamental to analyse the failure modes to identify possible alterations of the in-plane compressive features even if global results are satisfactory. As the samples showed through-the-thickness failures limited to the gage section, compliance for all the tested samples was confirmed.

3.2. Dynamic tests

3.2.1. Dynamic tensile test

The present test method presents multiple technical difficulties, as reported in paragraph 2.3.1 and in the related literature. As such, results shown in this paragraph have to be interpreted with reasonable uncertainty. Also, only one parameter is extracted, which is the tensile strength as function of the nominal strain rate. Results in terms of tensile strength and Specific Energy Absorption (SEA) are reported in Fig. 13, reporting average slopes of 0.30 MPa/s^{-1} and 0.015 (J/g)/s^{-1}.

3.2.2. Indentation test – D7136

As reported in Section 2.3.2, indentation was performed with three hemispherical impactors, of diameters 12.7, 16, 20 mm. Objective of the test was studying the performances of the fabric to different indenters at increasing energies; such performances were evaluated first by the comparison of the peak force and second by analysing the failure mode and damage. Energies chosen for the tests were in compliance to the will to evaluate the indentation behavior with a range of damage between a Barely Visible Impact (BVI), a Partial Penetration (PP) and Full Penetration (FP).

For all the three indenters, load cell results[2] reported ranges of peak forces between 2500 and 3500 N. However, no discernible trend was reported for the three impactors: the smallest showed peaks between 2750 and 3000 N, the intermediate between 2400 and 2700 N, the largest between 2750 and 3500 N. In terms of energy, Table 15 shows

[2] All the results were filtered with a 4-pole Butterworth at cutting frequency of 5 kHz.

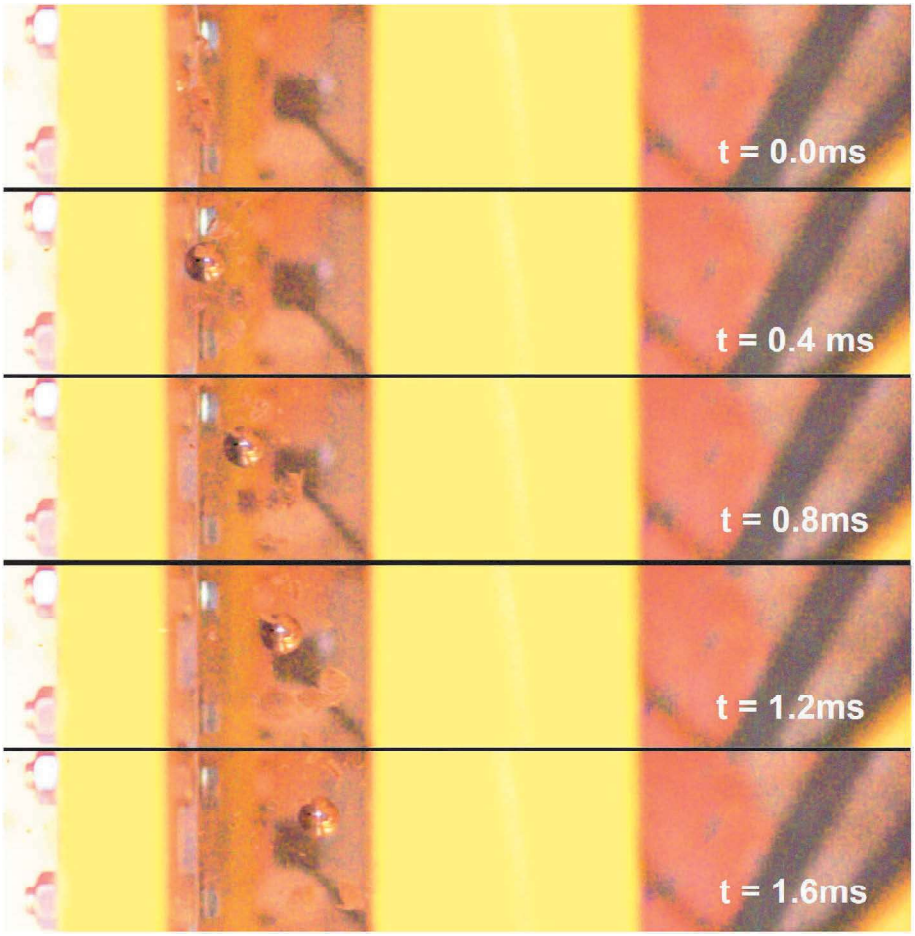

Fig. 17. Exit dynamics of the projectile and debris loss, sample 6: input speed 69.11 m/s, exit speed 39.68 m/s.

thresholds for Partial Penetration with fiber breakages between 10 and 20 J and a Full Penetration triggered between 25 and 30 J; both thresholds increased with the impactor diameters, reasonably expected as per the more distributed loading condition.

On the other hand, notable was an increase in the steepness of the force-displacement curve for increasing values of impact speed, as shown in Fig. 14. Such increase is calculated and plotted in Fig. 15, underlining consistently throughout the three impactors an increasing stiffness, measured as force over downward displacement. The stiffness was measured averaging force-displacement of the derivative values between 1000 and 2000 N, range found to be the most suitable to cancel out dynamic filtering effects present at the beginning of the curves. This effect, commonly found in impact and dynamic tests, consists in smoothing of the first elastic trait of the curve; it may be consequence of a low-pass filter applied to the raw signal, or determined by the bandwidth of the sensor: in this case, as the load cell bandwidth was 50 kHz, the filtering cut-off frequncy set at 5 kHz was likely the main cause of said effect.

In terms of failure mode and damage, for specimens with incomplete breakages a depression was exhibited in the front surface, with greater or lesser depth of penetration depending on the impact energy selected. The back surface was characterized by the presence of splits and cracks, which typical signs of delamination phenomena. It is worth noting that for higher impact energy tests splits occur in combined forms. Samples with complete failures were characterized by the presence of a gap in the center of the plate, in this case all the most common failure modes were exhibited: fiber breakage, fiber pullout, debonding and delamination phenomena. Little to none dispersion of debris following the impact was reported. Figures of the impacted specimens are reported in Section 3.2.4, Fig. 18, together with the post-impact pictures of the ballistic tests.

3.2.3. *High speed test*

Tests were peformed at range of muzzle speeds between 23 and 126 m/s, with the purpose of constructing the input-output speed curve, shown at Fig. 16. Results, collected in Table 16, reported a threshold speed of 47.2 m/s (energy 26.4 J) if interpolated between the two nearest experimental values, while speed of 46.7 m/s and energy of 25.8 J were identified by evaluating a second order polynomial fitting, reported in Equations (13) and (14).

$$v_{out}\ [m/s] = -0.01\ v_{in}^2 + 2.73\ v_{in} - 108.38 \tag{13}$$

$$E_{abs}\ [\%] = 0.01\ v_{in}^2 - 2.09\ v_{in} + 171.64 \tag{14}$$

In terms of failure mode, with respect to the indentation tests the failed specimens did not exhibit a longitudinal evolution of the crack; instead, visual inspection showed fiber breakage and pull-out due to the generation of high shear and bending stresses in the non-impacted side, as well as delamination phenomena. On the other hand, the fully penetrated samples reported a complete failure and the presence of a open hole after the impact. As for the low-speed indentation tests, although the fragmentation of the back surface could be seen during impact event, a limited amount of debris was generated (Fig. 17), which is a remarkable property in the context of crashworthiness applications where the minimization of debris plays a key role.

3.2.4. *Damage analysis for out-of-plane tests*

For the two test cases described at Sections 2.3.2, 2.3.3, 3.2.2 and

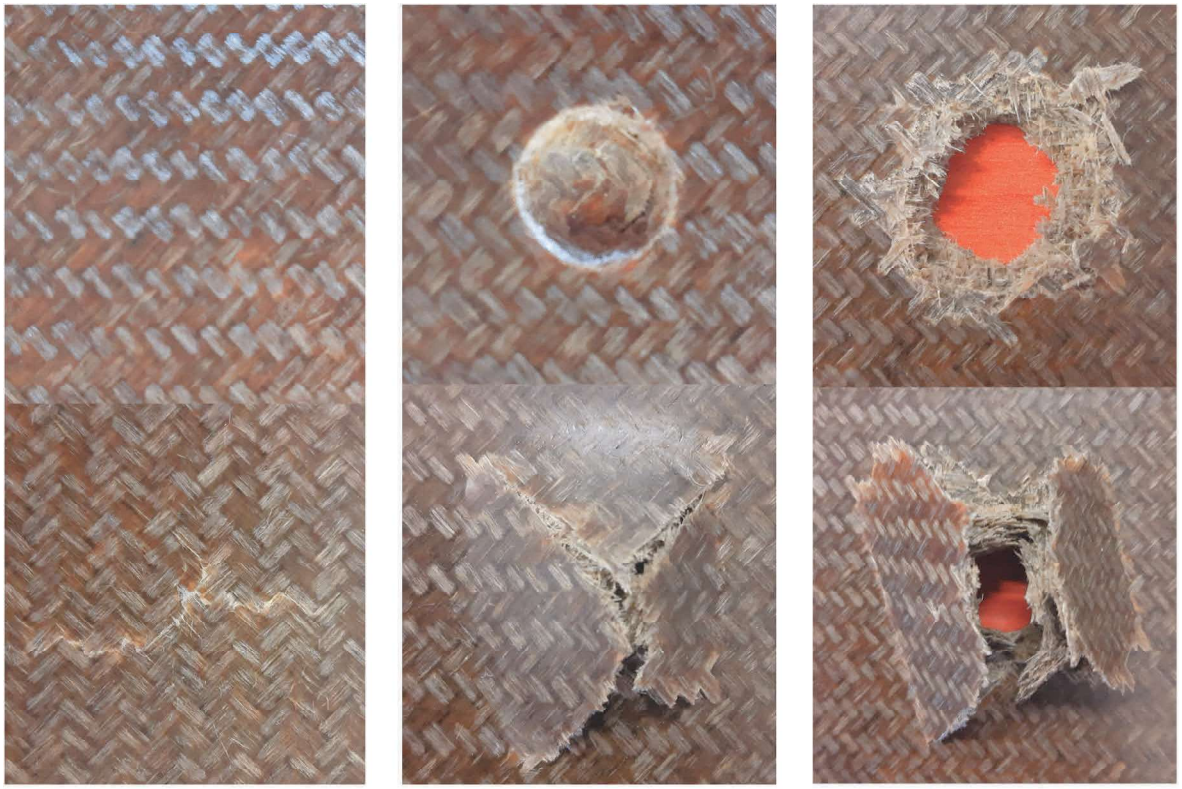

(a) Barely Visible (BV) damage (front and back surface)

(b) Partial Penetration (PP) damage (high and low speed, front and back surface)

(c) Full Penetration (FP) damage (high and low speed, back surface)

Fig. 18. Out-of-plane resistance – examples of damage types

Table 17
Threshold energy for out-of-plane tests. For the indentation with impactor of 16 mm diameter, no data of partial penetration was available; consequently, absorbed energy was calculated by averaging the loss of impact energy of the other impacts with the same indenter.

Test	Threshold impact energy [J]	Normalized threshold energy [J/mm^2]
Ballistics	25.8	0.12
Indentation D12.7	16.52 ± 2.75	0.11–.15
Indentation D16	16.48 ± 1.64	0.07–.09
Indentation D20	25.96 ± 3.33	0.07–.09

3.2.3, out-of-plane indentation/penetration resistance was further quantified by means of analysis of the failure region.

Visual inspection determined the definition of one or more predominant failure mode, of the visible extension of the damaged region and the damage type. As anticipated above, damage types defined, showed in Fig. 18, were the following: Barely Visible (BV), a slight dent on the impacted surface with no visible fibre cracking on the front surface and eventual crack on the back surface 18a; Partial Penetration (PP), hemispherical-shaped dent with clear fibre-crack dent with no penetration recorded 18b; Full Penetration (FP), with open holes and exposed delamination 18c.

It's worth noting that failure modes at low and high speeds were particularly different: the first were characterized, in all cases, by pronounced cracks, usually cross-shaped; the second feature much more localized damage, propagating radially from the impact centre.

However, Table 17 demonstrates thatpenetration thresholds in terms of energy were coherent, showing that strain-rate dependency is limited for a out-of-plane impact condition such as the one evaluated. Such feature is demonstrated by calculating the threshold energies and normalizing them with the resisting area: for the indentation analysis, the absorbed energy is calculated by means of integration of the force-displacement curve, for the ballistic analyses by means of input-exit speed calculation.

4. Summary and conclusions

In this work, a full characterization of the static, dynamic and impact properties of the flax-fiber composite Impregnatex APX 300T IMP503Z-HT BC 44 was carried out. The campaign included static tension, compression, shear and bending, dynamic tensile, low-speed indentation/penetration, ballistic tests.

The static tests campaign presented satisfactory results, and no improvements seemed to be needed. The composite showed high specific properties, of which the most significant are ultimate tensile stress of 181 MPa and Young modulus of 18 MPa. Peculiar mechanical properties were a bi-linear elasticity identified in the tensile tests and a considerable difference between 0° and 90° properties, higher than common values reported for standard syntethic composites. For what concerns the dynamic tensile tests, the machine hereby used showed sufficient reliability; being aware that accurate measurement of the strain is not achievable, force results reported reasonable coherence. The proposed method for specimen clamping, designed as alternative to non-effective standard solutions, showed great functionality and seemed promising for dynamic tests of material of similar stiffnesses (such as other natural or glass fiber composites): however, such method needs to be further validated, by variation of tested material and sample dimensions

together with measurement of the clamping force. The indentation/penetration tests were performed following the related standard, which confirmed its effectiveness in determining the resistance of the present composite; further analyses may be carried out variating thickness and lamination sequences, recording the debris dynamics during the impact, and analysing damage via non-destructive inspections. The ballistic campaign was purposely designed for the present work, and was meant to analyse the effects of a generic debris impact at high speed; outcomes were satisfactory and aligned with the low-speed results in terms of absorbed energy, excluding notable strain-rate dependency of the out-of-plane properties. Further studies may be carried out by employment of non-rigid projectiles, such as ice or bird-strike simulants, by variating their shape and dimensions and by considering different thicknesses and/or laminations sequences.

To conclude, the results achieved were positive, generally reporting consistency and coherence. Ultimately, the specific mechanical properties of the APX 300T IMP503Z-HT BC 44 can be compared to those of a glass fiber composite: commonly, such composites report ultimate stresses around 130 MPa/(g/cm^3) and Young moduluses around 12 GPa/(g/cm^3) [18], slightly lower with respect to the values here identified, 136 MPa/(g/cm^3) and 13 GPa/(g/cm^3) respectively. The in-plane strain-rate contribution was limited, 0.3 MPa/s^{-1}, while no discernible dependency was identified in terms of threshold energy in the out-of-plane impact tests; such results are aligned to composites of similar resins.

CRediT authorship contribution statement

Ivan Colamartino: Conceptualization, Investigation, Methodology, Writing - original draft, Writing - review & editing. **Elia Pinato:** Data curation, Methodology, Software. **Matteo Cavasin:** Methodology, Writing - review & editing. **Marco Tagliabue:** Methodology, Writing - review & editing. **Marco Anghileri:** Conceptualization, Project administration, Supervision. **Marco Boniardi:** Project administration, Supervision.

Declaration of competing interest

The authors declare the following financial interests/personal relationships which may be considered as potential competing interests:As authors Marco Tagliabue and Matteo Cavasin are, to submission date, employees of the company Angeloni Group, producer of the material under analysis, this poses a potential Conflict of Interest. It is here declared that all the results have been obtained as described in the paper, and by respecting Transparency and Ethics in Scientific Research. Furthermore, almost the full test activity was performed directly by Polytechnic of Milan, while Angeloni performed the samples' manufacturing and related post-manufacturing testing and quality assessment.

Data availability

Data will be made available on request.

References

[1] E.S. Stevens, Green Plastics: an Introduction to the New Science of Biodegradable Plastics, Princeton University Press, 2002.
[2] A. Gholampour, T. Ozbakkaloglu, A review of natural fiber composites: properties, modification and processing techniques, characterization, applications, J. Mater. Sci. 55 (3) (2020) 829–892.
[3] Layth Mohammed, M.N.M. Ansari, Grace Pua, Mohammad Jawaid, M. Saiful Islam, A review on natural fiber reinforced polymer composite and its applications, Int. J. Polym. Sci. 2015 (15) (2015), 243947, https://doi.org/10.1155/2015/243947L.
[4] O. Boegler, U. Kling, D. Empl, A. Isikveren, Potential of Sustainable Materials in Wing Structural Design, Deutsche Gesellschaft für Luft-und Raumfahrt-Lilienthal-Oberth eV Bonn, Germany, 2015.
[5] I. Elfaleh, F. Abbassi, M. Habibi, F. Ahmad, M. Guedri, M. Nasri, C. Garnier, A comprehensive review of natural fibers and their composites: an eco-friendly alternative to conventional materials, Results Eng. (2023), 101271.
[6] R.A. Eshkoor, S.A. Oshkovr, A. Sulong, R. Zulkifli, A.K. Ariffin, C.H. Azhari, Comparative research on the crashworthiness characteristics of woven natural silk/epoxy composite tubes, Mater. Des. 47 (2013) 248–257.
[7] M.A. Attia, M.A. Abd El-Baky, M.A. Hassan, T.A. Sebaey, E. Mahdi, Crashworthiness characteristics of carbon–jute–glass reinforced epoxy composite circular tubes, Polym. Compos. 39 (S4) (2018) E2245–E2261.
[8] J. Meredith, R. Ebsworth, S.R. Coles, B.M. Wood, K. Kirwan, Natural fibre composite energy absorption structures, Compos. Sci. Technol. 72 (2) (2012) 211–217.
[9] C.W. Isaac, C. Ezekwem, A review of the crashworthiness performance of energy absorbing composite structure within the context of materials, manufacturing and maintenance for sustainability, Compos. Struct. 257 (2021), 113081.
[10] Standard Test Method for Tensile Properties of Polymer Matrix Composite Materials, ASTM International, Standard, Dec. 2017.
[11] Standard Test Method for Compressive Properties of Polymer Matrix Composite Materials Using a Combined Loading Compression (Clc) Test Fixture, Standard, ASTM International (Mar., 2021.
[12] Standard Test Method for In-Plane Shear Response of Polymer Matrix Composite Materials by Tensile Test of a ±45° Laminate, ASTM International (Nov., Standard, 2018.
[13] Standard Test Methods for Flexural Properties of Unreinforced and Reinforced Plastics and Electrical Insulating Materials, ASTM International, Standard, Jul. 2017.
[14] M. Asim, M.T. Paridah, M. Chandrasekar, R.M. Shahroze, M. Jawaid, M. Nasir, R. Siakeng, Thermal stability of natural fibers and their polymer composites, Iran. Polym. J. (Engl. Ed.) 29 (2020) 625–648.
[15] Standard Test Method for Compressive Properties of Polymer Matrix Composite Materials with Unsupported Gage Section by Shear Loading, Standard, ASTM International (Mar., 2021.
[16] Standard Test Method for Measuring the Damage Resistance of a Fiber-Reinforced Polymer Matrix Composite to a Drop-Weight Impact Event, Standard, ASTM International (Nov., 2020.
[17] A. Abdullah, A. Khalina, A. Ali, Effects of fiber volume fraction on unidirectional kenaf/epoxy composites: the transition region, Polym.-Plast. Technol. Eng. 50 (13) (2011) 1362–1366.
[18] W. Chen, Q. Meng, H. Hao, J. Cui, Y. Shi, Quasi-static and dynamic tensile properties of fiberglass/epoxy laminate sheet, Construct. Build. Mater. 143 (2017) 247–258, https://doi.org/10.1016/j.conbuildmat.2017.03.074. https://www.sciencedirect.com/science/article/pii/S0950061817304464.